Image Processing for Measurement of Three-Dimensional GTA Weld Pool Surface

Hongsheng Song, Yuming Zhang*
Center for Manufacturing and Department of Electrical and Computer Engineering,
University of Kentucky, Lexington, KY 40506, USA
*: Corresponding Author Email: ymzhang@engr.uky.edu

Abstract

Observing and measuring the weld pool surface is a key to developing next-generation intelligent welding machines and to understanding the welding process better. In this paper, a dot-matrix pattern is used to project a commercially-available low power continuous laser onto the weld pool surface and the reflection of the laser is intercepted by an image plane which is placed with a distance from the arc. While the reflection of the laser travels without reducing much of the intensity, the intensity of the arc radiation decays with the distance rapidly. To utilize the reflection to reconstruct the weld pool surface, the correspondence of the reflection points with their projection points must be found. This paper addresses the algorithms to extract the reflection points from the image and then match the reflection points with their projection points. The establishment of the correspondence provides the data needed to reconstruct the weld pool surface based on the reflection law.

I. Introduction

Observation and measurement of weld pool surface provide an effective way to understand and control welding process. In recent years, different observation and measurement approaches have been developed, such as vision-based sensing techniques (Refs.1-4), ultrasonic technique (Ref.5), acoustic emission sensing technique (Ref.6) and thermal sensing technique (Ref.7). Especially for the vision-based sensing methods, they have evolved from two-dimensional (2D) to three-dimensional (3D) domain and are widely studied by many researchers. Accordingly some image processing work has been done to extract 2D geometry or 3D information of the weld pool surface (Refs.8-9). However, the dynamic and specular characteristics of weld pool surface and the interference of strong weld arc complicate the observation and image processing processes and affect the effectiveness of these methods.

In our previous work (Ref.1), a new three-dimensional observation system based on the reflection property of weld pool surface has been proposed. This system exploits the propagation difference between the welding arc and coherent structured laser light and turns the specular weld pool surface from an observation difficulty into an advantage. In the system, a structured laser pattern is projected onto the weld pool surface from the rear side at a certain angle, and an imaging plane is placed on the opposite side to intercept the laser

light reflected from the specular weld pool surface.

Different from existing approaches where the object to be imaged is directly viewed by a camera, the proposed approach views the reflection from the weld pool surface and resultant images are referred to as reflected images in this study. Its image processing is also different from those for existing approaches. Examples of images for 2D and 3D measurement from direct viewing approaches are shown in Fig.1. Usually by using image processing algorithms the boundary of weld pool can be extracted for 2D weld pool measurement and the distorted laser stripes can be identified to restore 3D weld pool surface. However, in our reflected images, only reflected laser dot-matrix pattern is captured and the boundary information is absent. Although such reflected images may also be extracted and interpreted by image processing algorithms to reconstruct the 3D weld pool surface, a survey shows that limited work has been done in this area for the reflected images. This paper thus devotes to the processing of reflected images for reconstruction of the weld pool surface.

In this paper, firstly the proposed observation system is presented and the observation results using different laser projection patterns are discussed in section II. Then correspondence simulation is conducted to illustrate possible correspondence relationships between projected and reflected laser dot-matrix patterns in section III. In section IV, the scheme of reflected image processing is discussed, which includes the dot extracting and dot matching algorithms. Finally, the conclusion is drawn in section V.

II. Proposed observation system

II.1 Observation system

The proposed weld pool sensing system is shown in Fig.2 (Refs.1, 10). The welding process used is the gas tungsten arc welding (GTAW). To observe the three-dimensional weld pool surface, a 20 mW *StockerYale*'s *Lasiris*™ SNF laser at wavelength of 685nm with variable focus is used to generate structured light pattern, such as dot-matrix pattern in the figure. The laser pattern is projected onto the area under the torch electrode and covers the whole possible weld pool surface. During the welding process, the molten weld pool surface is just like a mirror and it can reflect the majority of the incident laser light. In order to intercept the reflected laser pattern, an imaging plane is placed at a known distance from the electrode. It can be as simple as a piece of glass attached with a grid paper. An OLYMPUS i-SPEED high-speed camera capable of taking from 60 to 33000 frames per second is used to the reflected images on the imaging plane. To minimize the influence of the arc, the camera is fitted with a band pass filter of 20 nm bandwidth centered at wavelength of 685nm.

There are basically two advantages for the proposed system. First one is to change the specular weld pool surface from an observation difficulty to an advantage by exploiting the difference between propagation in illumination laser and arc plasma. The second is that the law which governs the measurement mechanism is simply the reflection law.

II.2 Projection pattern

In order to effectively reconstruct three-dimensional weld pool surface using reflected

images, the projected laser pattern should have some special characteristics to ease the processing. In our system, both commercial and customized laser diodes with different projection patterns are considered. Through investigation, there are two kinds of suitable laser patterns available commercially from *StockerYale* company. One is multiple-line pattern and the other is dot-matrix pattern.

In one of the experiments, a five-line structured light pattern (model SNF-505L(0.23)-685-20-5) is used and five parallel laser lines are projected onto the weld pool surface. Fig.3 (a) shows a clear reflected image in which the laser lines have been shaped by the weld pool surface. Although the deformation of weld pool can be easily recognized by the shaped lines, it is still difficult to use the reflected lines to reconstruct the surface due to the uncertainty of the correspondence of a particular point on a line to its incident ray.

The image in Fig. 3(b) is the reflection of a 19*19 dot-matrix projection pattern (model SNF-519X(0.77)-685-20) from the weld pool surface. Although the area covered by the pattern is larger than weld pool area, only the dots projected on the weld pool surface can be reflected on the imaging plane. The intensity and contrast of the reflected dots are not as strong as that in Fig.3 (a), but as will be shown later the reflected dots can still be processed to extract the reflected dots for analysis. In addition, combined with the results of correspondence simulation to be discussed later, the reflected points can be matched with their corresponding projection points in the dot matrix one by one. As a result, the reflection law will be able to be used to compute the weld pool surface.

For dot-matrix projection, an appropriate image processing technique that can effectively match the reflection points with their projection points is crucial. To ease the matching, customized projection patterns with different specially-designed symbols may help. However, because the reflected symbols may change from their projection shapes, their recognition may still be difficult. For easy implementation by other researchers, the authors decided to use the commercially available 19*19 dot-matrix pattern. As mentioned above, an appropriate image processing technique now becomes a major step toward successful reconstruction of weld pool surface.

II.3 Observation results

In a typical experiment using the dot-matrix laser pattern, 2 mm thick mild steel sheet was used as the work piece. The welding current was kept at 70 Amp, and the welding speed is 2 mm/s. The 19*19 dot-matrix laser pattern is projected onto the weld pool surface under the torch electrode at 30 degree in YOZ plane and the inter-beam angle is 0.77 degree. The distance from the laser to the weld pool is approximately 40 mm. An imaging plane is parallel to the XOZ plane at a known distance of 49 mm from the axis of the electrode. Fig.4 shows four images acquired sequentially. From the images, one can clearly see the reflected dots. The pattern has been distorted by the specular weld pool surface.

Moreover in Fig.5 (a), one can find that the center point (in 10^{th} row and 10^{th} column) in the projected dot matrix is absent, which can be used to help to locate the position of reflected dots as a reference. In Fig.5 (b), the position of the reference point is shown.

From above observation results, it is apparent that clear images can be acquired using the proposed approach with a low-power continues illumination laser. The acceptable

clearness of the images assures that they can be processed to accurately extract the laser dots shaped by the specular weld pool surface and thus be used to accurately compute the weld pool surface.

III.Correspondence simulation

The similarity of the dots in the reflected image makes it difficult to tell the exact incident rays they come from. Simulation is thus conducted in order to find the possible correspondence relationships between the projected and reflected laser points.

III.1 Correspondence relationships

In the simulation, there are mainly two kinds of corresponding relationships for the dot-matrix pattern, which are shown in Fig.6 (The axes show the view plane). One is the correspondence of dots in a line, and the other is the correspondence of lines in a dot matrix. They both have three types of mapping according to different shapes of reflection surface: sequential, inverse and disordered.

Fig.4 shows a typical reflected image acquired, and thus the shape of reflected dots in a line is convex as shown in Fig.6 (a). Here a line with 7 dots is used as an example. The dash lines indicate the correspondence relationships between projected and reflected points. In "inverse" mapping, the middle point is the center of inversion, such as the point 4 in Fig.6 (a).

In Fig.6 (b), three types of mapping of lines' correspondence relationships are shown, and the numbers present different projected rays in different lines. The differences among these types of mapping are caused by different statuses of weld pool surface, such as shallow or deep, concave or convex.

III.2 Simulated surfaces

In the simulations, a part of sphere is used as a simple concave or convex weld pool surface in Fig.7. Here ***r*** is half of the width (length) of the weld pool surface and ***d*** is its depth. Some other numerical models of weld pool surface may also be applied in the simulation, such as the one in (Ref.11). Since only the correspondence relationships are investigated in the simulation, these two simulation surfaces are representative.

III.3 System parameters

In the simulations, some system parameters are set according to above proposed system experiment in section 2.3. The distance between imaging plane and torch is 49 mm, and the horizontal distance between Laser and torch is 40 mm. For the laser diode, the projection angle is 30 degree.

For GTAW, the dimensions of the weld pool surface are typically 5 mm in width, 6 mm in length, and 0.5 mm in depth if the current is below 150A as used for precision joining (Ref.12). According to previous study, the values of parameters in the correspondence simulation are designed. First, different sizes of weld pool are investigated and the value of r in Fig.7 is changed from 2mm to 5mm. Second, the depth d is also changed from r/10 to r/5, which is associated with the width.

III.4 Simulation results

MATLAB is used as the programming language to simulate the proposed system. And above system parameters are used for both concave and convex surfaces.

Simulations show that for concave surfaces, the shapes of reflected images are all convex and the correspondence relationships of dots and lines are all inversed. For convex surfaces, the correspondence relationships of dots and lines are all sequential and all the reflected images are convex.

As can be seen, only regular convex and concave surfaces are tested here. If the weld pool surface is irregular as it could be in plasma keyhole arc welding or laser keyhole welding, the third corresponding relationship 'disordered' as shown in Fig. 6 may occur. If this does occur, one will not be able to determine the correspondence between projected and reflected dots using the proposed process. In such a case, one may use two facts/constraints to determine the optimal matching through computation and comparison: (1) the number of the dots is finite; (2) the weld pool surface is smooth and meet certain shape constraints even though the slope may be large. Since the studied reflected images are recorded during GTAW with moderate currents, the weld pool surface is not severely deformed. In such a case, irregular reflected images are not found in our experiments. Hence, in this study, only regular convex and concave surface will be considered.

IV. Processing of reflected image

The flowchart for the image processing is shown in Fig.8. First of all, the reflected laser points in the image should be extracted based on their shape and size. Then based on the assumption that the deformation of the weld pool is small in GTAW so that the shape of reflected matrix does not deform severely, the reflected points are analyzed and some image features are determined, such as their row-column relationship and the position of reference point. Then the corresponding relationships discussed in section III can be applied to identify the corresponding projected point for each reflecting point in the image.

IV.1 Dot extracting algorithm

One of the reflected images acquired by the monochromic camera during experiment is shown in Fig.9. In the image, the whole imaging plane is captured and there are some white reflected points in the black background.

1. Reflected image segmentation

Image segmentation methods can be used to separate the reflected light dots from the background and noise. For the reflected image, one can also segment it into "reflected points" and "background" by simply choosing a threshold in brightness (Ref.13). The choice of grey level threshold is important for the success of reflected point extraction.

There are several ways to realize thresholding by using proper threshold, ranging from the trivially simple to the very sophisticated. In our experiment, in order to balance the effect of segmentation and the real-time speed, a local thresholding approach called "block thresholding" is selected, in which the picture is partitioned into rectangular blocks and different thresholds are used on each block (Ref.13). Let R present the entire image region,

and R is partitioned into n subregions, R_1, R_2, R_3 .....R_n as shown in Equ.1.

Since the size of acquired images in the proposed system is 480*640 (pixel), **40*40** is chosen as the size of each block R_i for thresholding which is found to be able to balance speed and output results. And for each subregion R_i, a different threshold is R_i is applied to segment the subimage, which is shown in Equ.2.

Here a simple strategy is chosen to find the threshold, which is to average the intensity in each block and choose the average intensity $\overline{I}_i$ plus ΔI as the threshold, just as shown in Equ.3.

Where ΔI is a small increase of intensity, and **5** is selected for 256 grey levels in our application. In Fig.10, the result is shown. After the segmentation, the input image becomes a binary image.

2. Background noise reduction

There are still some noises in the image after the segmentation. The next step is thus to delete the background noises. Here two-level noise reduction operations are used.

In image processing technology, median filters are particularly effective in the presence of impulse noise, also called salt-and–pepper noise because of its appearance as white and black dots superimposed on an image (Ref.14). Here considering the small size of majority of the noises, **3*3** median filter is chosen for the first level noise deletion.

After using median filter, there are still some relatively large noises (in comparison with the impulse noise) in the image. Hence in the next step, the average size of the dots in Fig.10 is calculated as Equ.4.

Here *m* is the number of dots in the image and S_i presents the size of the i^{th} dot in the image (unit: pixels). $S_a/6$ is selected based on experimental results as the threshold to delete the dots with smaller size which are considered to be noises. The operation can be expressed as Equ.5.

Here $f(x,y)$ is the intensity of a pixel in the image after using median filter and D_i presents the area of the i^{th} dot. After this operation the big size noise dots (which left in the image after filtering with the median filter) and interference dots can be eliminated as shown in Fig.11.

3. Dots shaping using morphological operations

Due to the uneven intensity within reflected points in image, sometimes one reflected point may have been divided into several parts after segmentation, which can be seen from Fig.11. In order to reconnect the separated parts of the dots, some morphological operations should be done. One possible way is to dilate the dots in the image both in vertical and horizontal direction. After analyzing the features of the separated dot parts, the average length L_a and average width W_a of the dots in Fig.11 are computed as Equ.6 and Equ.7.

Here *n* is the number of dots in the image shown in Fig.11 and D_i presents the area of the i^{th} dot. And L_a and W_a are used as the length of vertical and horizontal structuring element vectors for dilation. And the result of dilations is shown in Fig.12. As can be seen,

the separated parts of one reflected dot are reunited, which greatly improve the quality of the image.

4. Determination of the reflected points' position

In this step, the center pixel position of each dot is calculated to precisely present its position in the image coordinate system, as shown in Equ.8.

Here *m* is the number of dots and n_i present the number of pixels in the i^{th} dot. And $(x_i \quad y_i)$ present the calculated position of the i^{th} reflection dot in the image. Fig.13 shows the positions of the reflected dots in image coordinate system.

IV.2 Dot matching algorithm

Once the reflected laser points are extracted from image and their positions are calculated, the following task is the characteristics identification. One is to decide position relationship of reflected points. And the other is to locate the position of the reference point. During these processes, imaging plane coordinates are used in the algorithm, shown in Fig.14.

This is a kind of pattern recognition problems, which may be solved by some existing algorithms. In order to simplify the processing procedures for our case, a new dot matching algorithm is developed. The main procedures of position and characteristic identification are discussed below.

1. Row position analysis

For a pair of dots, there are mainly two parameters used to describe their relative positions. One is distance, and the other is the angle of their connected line. They are all important for the decision of row/column relationship among the reflected dots. Through analysis, it is found that the distance plays more important role in deciding the row relationship and the angle is more important for column relationship in the reflected images.

The procedures of row searching algorithm are shown in Fig.15. Firstly an available reflected point set R is built. Then the rows of reflected points are searched one by one. At first, beginning point of each row is selected, which is located on the most left position within set R. Then its right neighbor in the same row is found by searching for the nearest point. The search of points in the same row is continued until the row angle conditions (row angle is less than 60 degree and change of row angle is less than 90 degree) are not satisfied, which indicates the end of this row. Then begin to search for the next row until all the dots are categorized into particular rows.

Here the row angle of a dot is defined as the angle of line connected this dot and its left neighbor point and the x-axis of imaging plane coordinate system, which is shown in Fig.16. And the beginning point of each row has no row angle, such as point A. As can be seen in Fig.17, five rows are found by the row searching algorithm, which verified the accuracy of the method.

2. Column position analysis

The next step is to decide the column position for each point in the rows. The main idea is to find the row with the most points and assign the column number from left to right. Then using this row as a reference, the column position of the points of its neighbor rows (below or

above it) can be decided by column angle. Hence through one by one search, the column positions of points in all rows can be determined. The procedures of column searching algorithm are detailed in Fig.18 and are not repeated here.

Here the column angle of a dot is defined as the angle formed by the line connecting this dot and a dot in its neighbor row with the x-axis, which is shown in Fig.19. The result of column searching is shown in Fig.20.

3. Blocked row marking

In the welding process, the torch blocks some reflected laser dots in a row, which should be identified. After the column position of each point is decided, it is easy to judge row integrity. The columns of three middle points in the row with the most points are considered as reference columns. If there is more than 1 point in a row not locating in these columns, this row is marked as blocked row and may not be used for computation of weld pool surface.

4. Reference point determination

This refers to find the row with one missing center column point. If two or more rows are available, the row with missing point in the center is chosen. The position of the missing point should be corresponding to the center position (10th row and 10th column) in the projection 19*19 dot matrix. Thus the reference point can be found, as shown in Fig.21.

IV.3 Result analysis

After the image processing, the relative row and column position is decided for each reflected laser point, just as shown in Fig.22 (a). For example, the points B, C and D belong to 4^{th} row and the points E, C and F locate in 3^{rd} column. And the position of reference point can be found in the circled area A, which is corresponding to the 10th row and 10th column absent point in the projected 19*19 dot matrix.

If the corresponding relationship discussed in section III is known, the absolute reflection position for each reflected point can be further determined, which means one can tell a reflected point is reflected from which point in the projected dot matrix. In Fig.22 (b), the different results of absolute positions are shown according to different correspondence relationships. For example, if the dots and lines correspondence relationship are both sequential (S/S), point C is reflected from the projected point at 11^{th} row and 6^{th} column in the 19*19 dot matrix. If the correspondence relationships are both inverse (I/I), it is reflected from the point at 9^{th} row and 14^{th} column. These possible correspondence relationships can be used later in the computation of the weld pool surface.

V. Conclusions

This paper focuses on the development of algorithms for processing the image of a dot-matrix laser pattern reflected from the weld pool surface in order to obtain the data needed to reconstruct the weld pool surface based on the reflection law. The authors found:

- The proposed system which projects a pattern of a low power continuous laser on the weld pool surface and intercepts the pattern's reflection from the weld pool surface provides an effective method to image the specular weld pool surface;
- The dot-matrix pattern used provides an acceptable method to successfully establish the reflection-projection correspondence needed to reconstruct the weld pool surface.

It reduced the image contrast but eased the point matching;

- The proposed dot extracting algorithms are capable of extracting the reflection points from the image with reduced contrast;
- The proposed dot matching algorithms can successfully match the reflection points to their projections points;
- The proposed use of laser reflection and dot-matrix pattern and the proposed image processing algorithms including the dot extracting algorithms and dot matching algorithms form a system of solutions to acquire the data which can be used to compute the specular weld pool surface based on the reflection law.

Acknowledgement

This research is funded by the National Science Foundation under Grant DMI-0527889 “Sensors: Measurement of Dynamic Weld Pool Surface.” Hongsheng Song also thanks the University of Kentucky Graduate School for the financial support through the Kentucky Opportunity Scholarship.

Reference

1. Y.M. Zhang, H.S. Song, and G. Saeed, 2006, “Observation of a dynamic specular weld pool surface,” MEASUREMENT SCIENCE & TECHNOLOGY 17 (6): L9-L12.
2. 2. R. Kovacevic, Y. M. Zhang, and S. Ruan, 1995, "Sensing and control of weld pool geometry for automated GTA welding," ASME Journal of Engineering for Industry, 117(2): 210-222
3. Mnich, C., Al-Bayat, F., Debrunner, C., Steele, J., Vincent, T., 2004, “In Situ Weld Pool Measurement using Stereovision”, ASME, Proceedings 2004, Japan – USA Symposium on Flexible Automation, Denver, Colorado, July 19-21
4. C. S. Wu, P. C. Zhao, and Y. M. Zhang, 2004, “Numerical simulation of transient 3-D surface deformation of full-penetrated GTA weld pool,” Welding Journal, 83(12): 330s-335s
5. Siores, E., 1988, “Development of a realtime ultrasonic sensing system for automated and robotic welding”, PhD Thesis, Brunel University
6. Groenwald, R. A., Mathieson, T. A., Kedzior, C. T. and Gaid, I.N.C., 1979, “Acoustic emission weld monitor system – data acquisition and investigation”, US Army Tank-Automotive Research and Development Command Report ADA085-518
7. Chin, B.A., Madsen, N.H. and Goodling, J.S., 1983, “Infrared thermography for sensing the arc welding process”, Welding Journal, Vol. 62 No. 9, pp. 227s-34s.
8. Kovacevic, R., Zhang, Y.M. and Ruan, S., 1995, “Sensing and control of weld pool geometry for automated GTA welding”, ASME Journal of Engineering for Industry, Vol. 117, No. 2, pp.210–222.
9. R. Kovacevic, Y. M. Zhang, 1997, "Real-time image processing for monitoring of free weld pool surface," ASME Journal of Manufacturing Science and Engineering, 119(2): 161-169
10. Hongsheng Song, Gohar Saeed and YuMing Zhang, 2006, “Observation of Dynamic Specular Weld Pool Surface”, Proceedings of 2006 ISFA (International Symposium on

Flexible Automation), 0252-b(S) pg.661-662, Osaka, Japan, July 10-12
11. Saeed G., Lou M. J., and Zhang, Y. M., 2004, "Computation of 3D weld pool surface from the slope field and point tracking of laser beams". Measurement Science and Technology, 15(2): 389-403
12. Mingji Lou,"Computation of Weld Pool Surface from Specular Reflection and Optical Flow", Master Thesis, University of Kentucky, 2004
13. Wesley E. Snyder and Hairong Qi, 2004, "Machine Vision", Cambridge University Press, ISBN 052183046X
14. Rafael C. Gonzalez, Richard E. Woods, 2002, "Digital Image Processing", second edition, Prentice Hall,

$$\bigcup_{i=1}^{n} R_i = R \qquad \text{…… (Equ.1)}$$

$$f_i(x,y)=\begin{cases}1 & if\,..R_i(x,y)>T_i \\ 0 & if\,..R_i(x,y)\le T_i\end{cases} \quad i=1,2,....n \qquad \text{…… (Equ.2)}$$

$$T_i=\bar{I}_i+\Delta I\ ,\ i=1,2,....n \qquad \text{…… (Equ.3)}$$

$$S_a=\left(\sum_{i=1}^{m}S_i\right)\Big/m \qquad \text{…… (Equ.4)}$$

$$g(x,y)=\begin{cases}1 & if\,..(x,y)\in D_i\,..and\,..S_i>(S_a/6),..i=1,2,..m \\ 0 & if\,..(x,y)\in D_i\,..and\,..S_i>(S_a/6),..i=1,2,..m \\ f(x,y) & otherwise\end{cases} \qquad \text{…… (Equ.5)}$$

$$\begin{cases}L_a=\left(\sum_{i=1}^{n}L_i\right)\Big/n \\ W_a=\left(\sum_{i=1}^{n}W_i\right)\Big/n\end{cases} \qquad \text{…… (Equ.6)}$$

$$\text{where}\ \begin{cases}L_i=\max\{y\,|\,(x,y)\in D_i\}-\min\{y\,|\,(x,y)\in D_i\} \\ W_i=\max\{x\,|\,(x,y)\in D_i\}-\min\{x\,|\,(x,y)\in D_i\}\end{cases} \ i=1,2,...n \qquad \text{…… (Equ.7)}$$

$$\begin{cases}x_i=\sum_{k=1}^{n_i}x_{ik}\Big/n_i \\ y_i=\sum_{k=1}^{n_i}y_{ik}\Big/n_i\end{cases} ,.....(x_{ik},y_{ik})\in D_i\,and\,..i=1,2,...m \qquad \text{…… (Equ.8)}$$

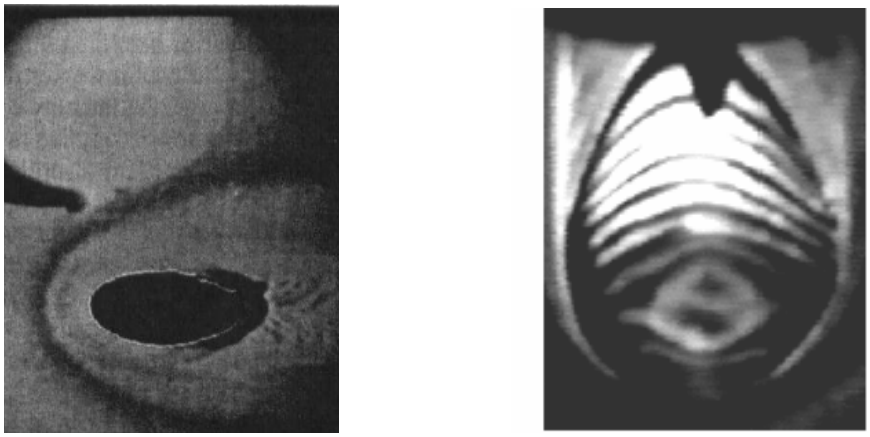

Fig.1. Example Images for (a).2D measurement (Ref.8) and (b).3D measurement (Ref.9)

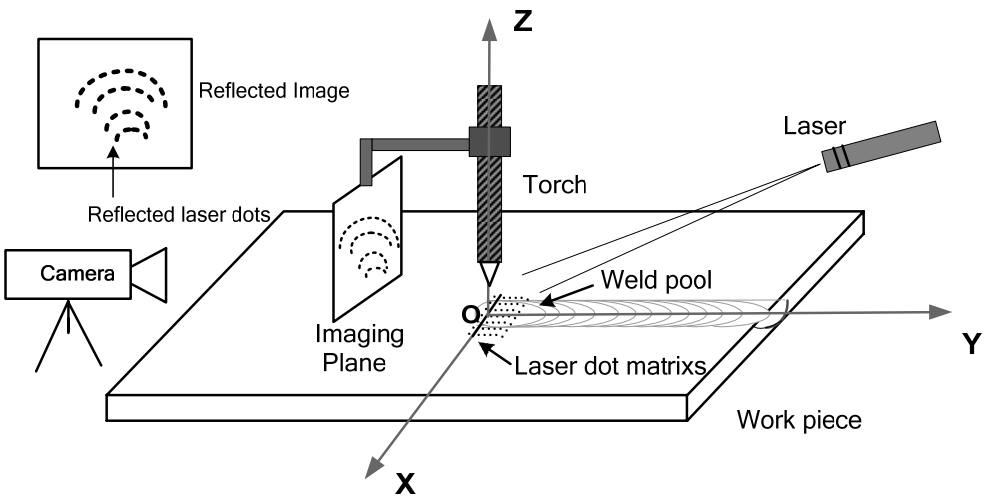

Fig.2 System Diagram

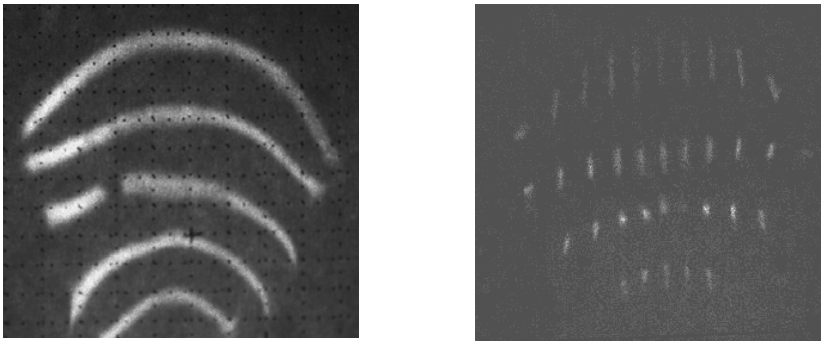

Fig.3 Reflected image using a (a) five-line laser projection pattern (b) 19*19 dot-matrix laser pattern

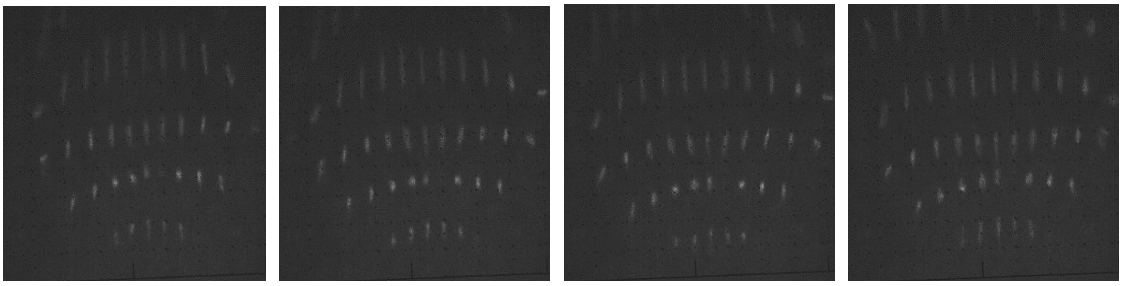

Fig.4 Acquired reflected images

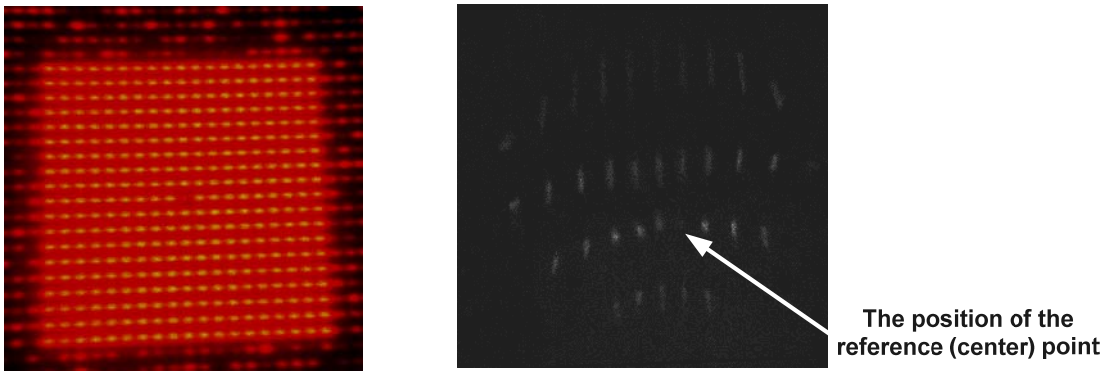

Fig.5 Reference point in (a) projected dot matrix and (b) reflected image

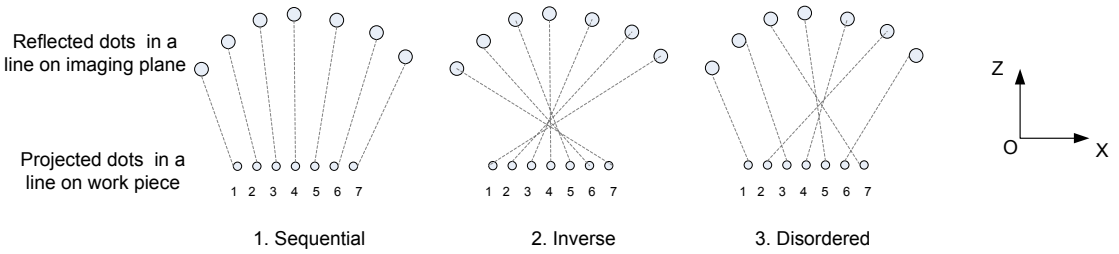

(a) Correspondence relationships of dots in a line

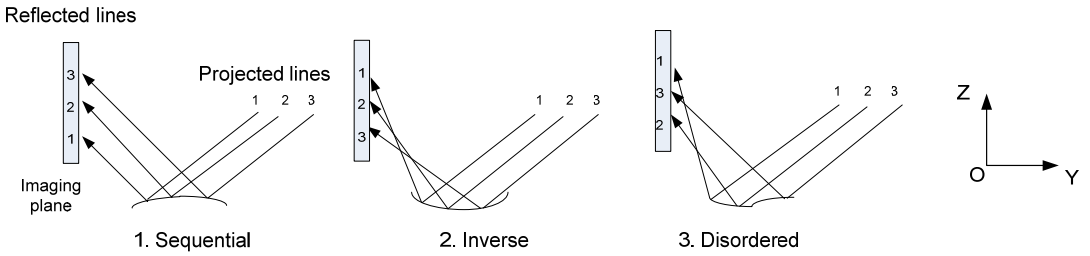

(b) Correspondence relationships of lines in a dot matrix

Fig.6 Two kinds of correspondence relationships

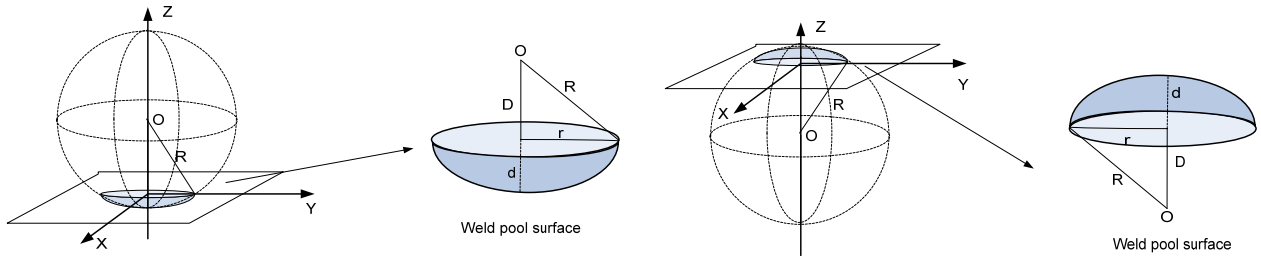

(a) Concave simulation surface (b) Convex simulation surface

Fig.7 Two simulation surfaces

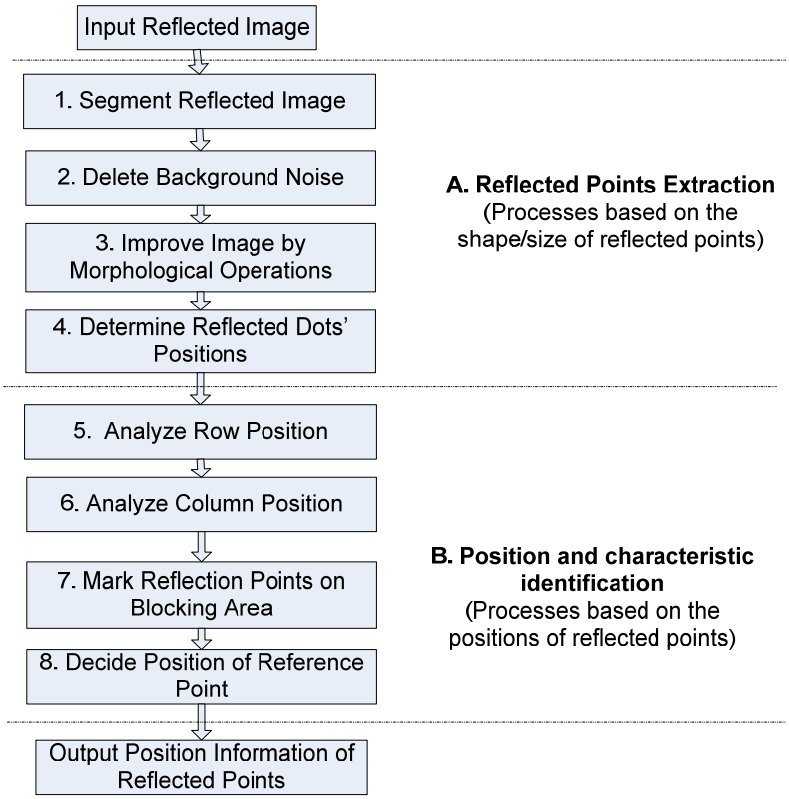

Fig.8 Flowchart for image processing

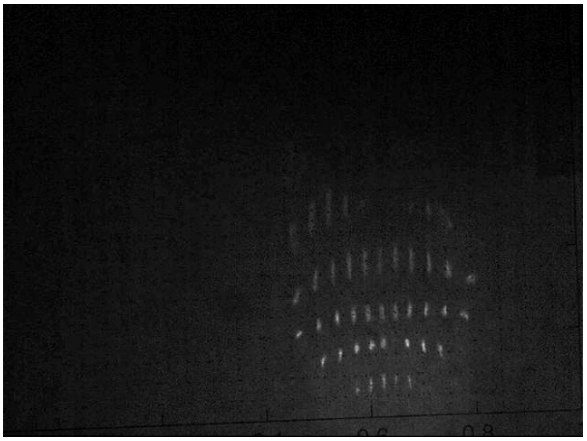

Fig.9 Captured reflected dot-matrix image

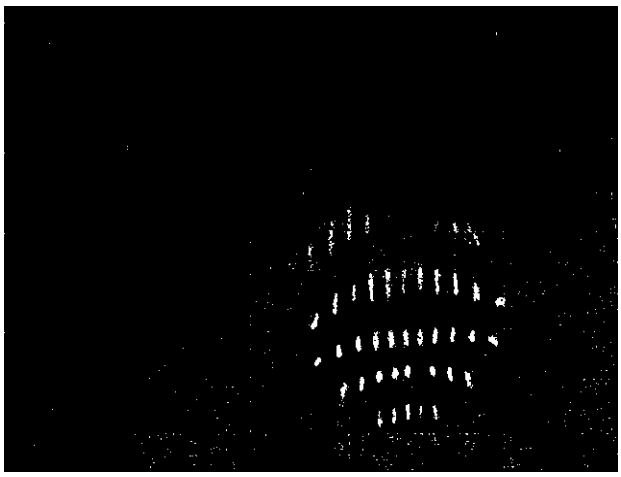

Fig.10 Block thresholding result

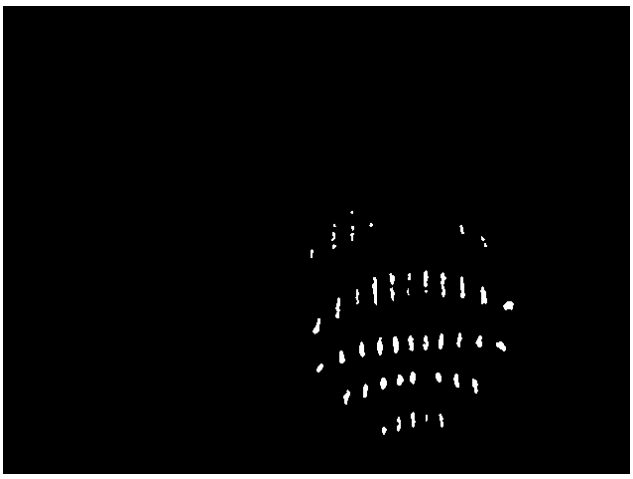

Fig.11 Results of two-level noise deletion

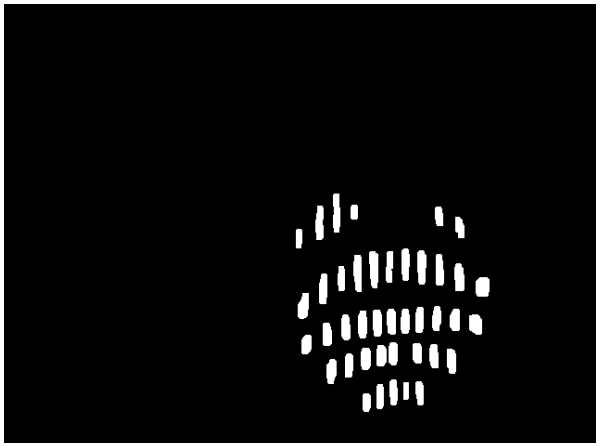

Fig.12 Results of dots dilation

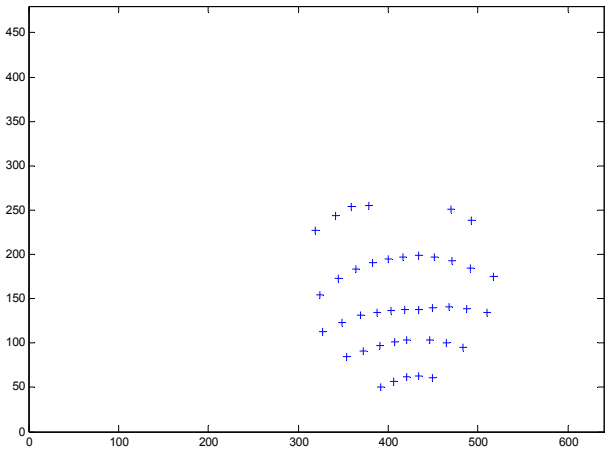

Fig.13 Position determination

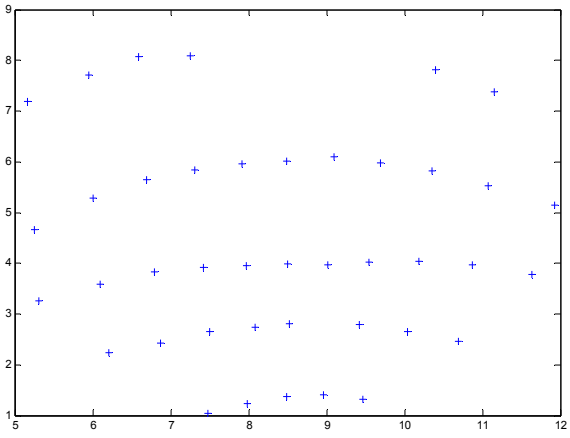

Fig.14 Reflected points (imaging plane coordinates)

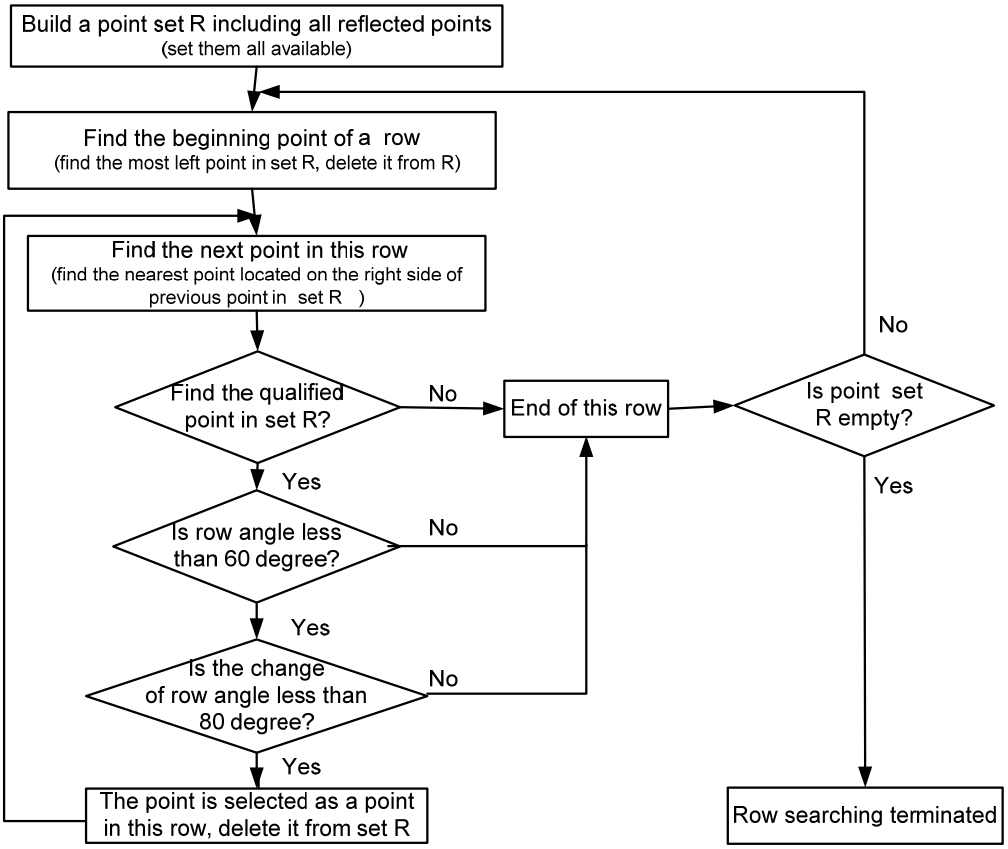

Fig.15 Flowchart of row searching

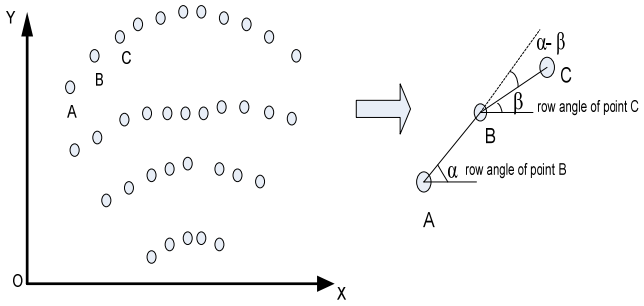

Fig.16 Row angle illustration

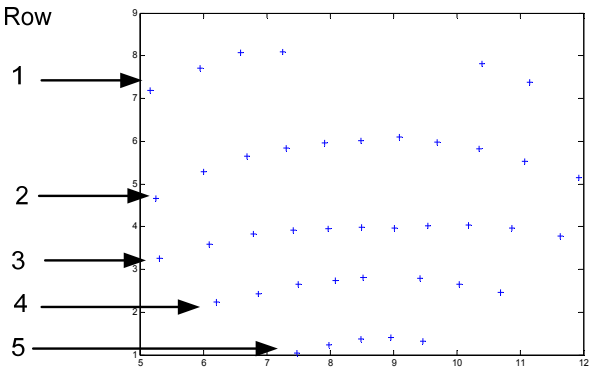

Fig.17 Result after row searching

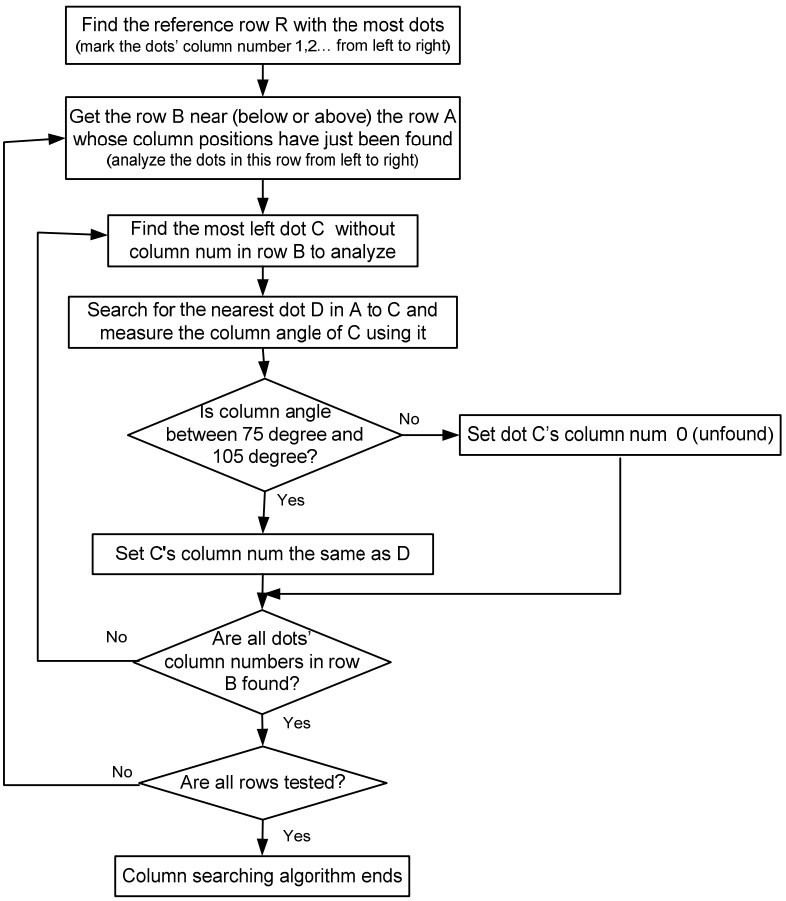

Fig.18 Flowchart of column searching

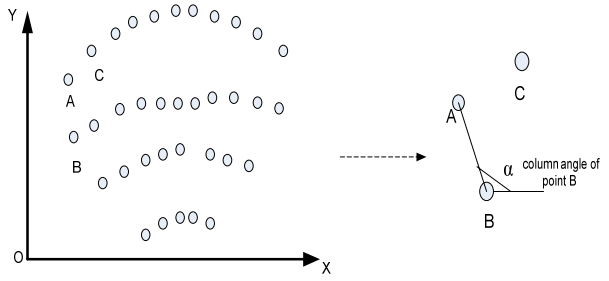

Fig.19 Column angle illustration

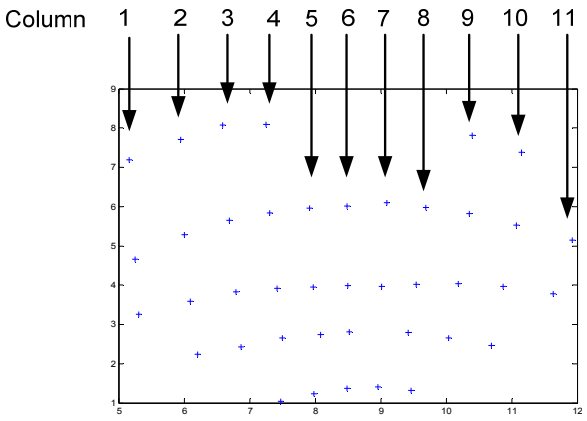

Fig.20 Result after column searching

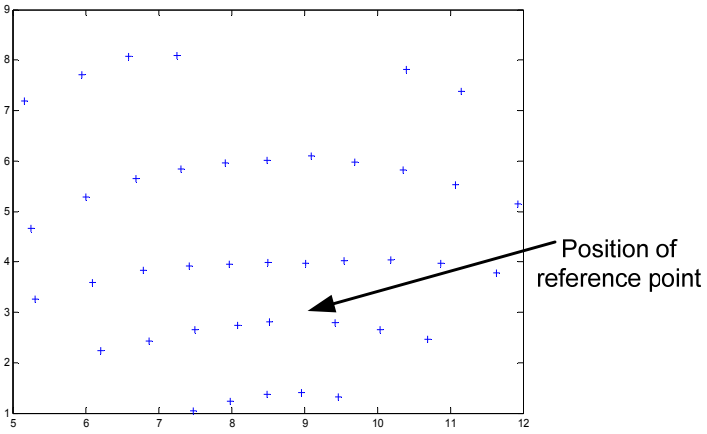

Fig. 21 Position of reference point

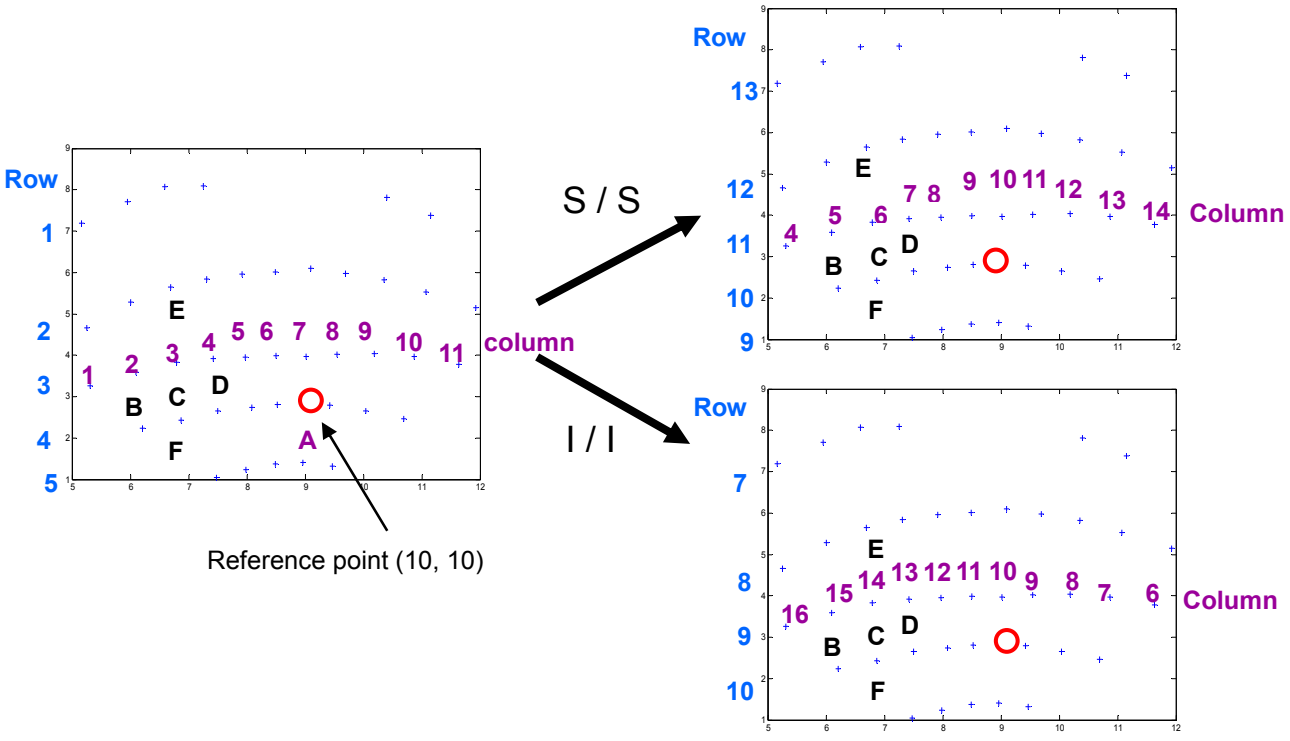

(a). Relative positions after image processing (b). Absolute positions with correspondence relationship

Fig.22 Illustration of correspondence relationship between projected and reflected dots